Journal of Solar Energy Research (JSER)

Journal homepage: www.jser.ut.ac.ir

A Novel Fan-Based Cooling System for Photovoltaic Panels: Impact on Thermal Regulation and Electrical Efficiency

Alireza Asgharzadeh Karamshahlu, Hooman Bahman Jahromi, Mohammad Hassan Saidi*

Center of Excellence in Energy Conversion (CEEC), School of Mechanical Engineering, Sharif University of Technology, Tehran, Iran

ARTICLE INFO

Article Type:

Research Article

Received:2025.12.04
Accepted in revised form:2026.02.03

Keywords:
Photovoltaic cooling system;
Suction-based airflow Forced convection;
Thermal management;
Temperature uniformity;
Electrical efficiency

A B S T R A C T

This study experimentally investigates a suction-based fan cooling system to improve the thermal and electrical performance of photovoltaic (PV) modules under outdoor conditions. Low-power axial fans extract heated air from a sealed plenum behind the panel, inducing distributed inflow through inlet holes. This limits warm-air recirculation and creates uniform convective streams across the backside. Experiments were performed on a clear, sunny day with a peak irradiance of 1030 W/m² and an ambient temperature of 32 °C. The system achieved a maximum surface-temperature drop of 15.5 °C relative to an uncooled module. With the experimental results subjected to a rigorous uncertainty analysis, infrared thermography confirmed a more uniform temperature with no visible hot spots. Electrical performance was assessed using a 15-minute duty cycle (5 min ON / 10 min OFF) to balance cooling and auxiliary energy use. Based on the manufacturer's temperature coefficient combined with measured surface temperature and irradiance, the system yielded an estimated net electrical efficiency gain of 0.94% after accounting for fan consumption. Compared with conventional rear-side blowing, the suction architecture demonstrated superior cooling, improved thermal uniformity, and potentially better long-term stability, offering a compact, energy-efficient solution for PV modules in warm climates.

1. Introduction

The rapid expansion of photovoltaic (PV) technology has made it a cornerstone of renewable energy, yet elevated operating temperatures significantly reduce electrical efficiency, typically by 0.3–0.5% per °C rise [1]. Consequently, effective thermal management has attracted extensive research attention. Cooling strategies reported in the

*Corresponding Author Email: saman@sharif.edu

Cite this article: Asgharzadeh Karamshahlu, A., Bahman Jahromi, H. and Saidi, M. H. (2026). A Novel Fan-Based Cooling System for Photovoltaic Panels: Impact on Thermal Regulation and Electrical Efficiency. Journal of Solar Energy Research, 11(1), 2767-2779. doi: 10.22059/jser.2026.407563.1679

DOI: 10.22059/jser.2026.407563.1679

literature can be broadly classified into passive, active, and hybrid approaches.

Passive cooling techniques, including water-based systems, phase change materials (PCMs), heat sinks, and heat pipes, primarily aim to dissipate excess heat without auxiliary power. Water or PCM layers integrated into PV structures have demonstrated notable temperature reductions and substantial improvements in electrical output [2,3], while customized passive configurations, such as cooling towers, reduced panel temperatures from 50 °C to 30 °C, improving annual efficiency by around 7% [4]. Similarly, heat sinks and heat pipes have effectively mitigated thermal stresses and improved reliability, with optimized fin geometries and novel perforated or wavy structures further enhancing dissipation [5-8]. Despite these benefits, passive methods often exhibit delayed responses to fast-changing irradiance and may suffer from material-related issues, such as PCM leakage and higher costs [9-13].

Active cooling approaches focus on enhancing convective heat transfer. Forced-air systems, such as ducted PV façades or rear-mounted fans, have achieved temperature reductions of up to 25 °C and measurable gains in electrical output [14,15]. Liquid-based strategies, including sprinkler and evaporative air cooling in PV/T systems, also demonstrated significant effectiveness under hot climates [16,17]. However, fan-assisted approaches often yield only limited improvements in average cell temperature and may still exhibit non-uniform thermal fields due to recirculation or uneven airflow distribution, thereby restricting long-term performance gains [18,19].

Hybrid concepts combine two or more mechanisms to maximize heat removal. Examples include thermoelectric generators integrated with dual-axis tracking, achieving efficiency improvements from 10.6% to 14% [20], or systems combining active convection with PCMs to maintain a stable cell temperature under fluctuating radiation [21]. Advanced frameworks combining PCMs, nanofluids, heat pipes, thermoelectric modules, and assisted airflow have demonstrated synergistic cooling performance [22-24], with reported temperature reductions up to 31% and power gains as high as 67%, depending on the technique [25]. Nonetheless, reviews consistently indicate that no single solution is universally optimal; performance depends on climatic conditions, cost, and auxiliary power consumption [26,27].

Experimental investigations highlight the potential of PCM integration to maintain nearly constant cell temperature and to improve energy output under high irradiance [28], while forced-convection studies demonstrate significant reductions in PV temperature and improvements in performance under various operating conditions [29].

Despite the wide range of passive, active, and hybrid cooling techniques reported in the literature, most approaches primarily reduce the mean operating temperature while providing limited suppression of in-plane temperature gradients at the module surface. Such gradients promote localized hot spots, induce differential thermal stresses, and accelerate material degradation, ultimately constraining the long-term performance of PV modules [18]. In addition, fan-based air-cooling configurations commonly rely on backside blowing through open ducts, which can favor recirculation of heated air and lead to uneven convective action. As a result, the resulting thermal improvements tend to be modest and spatially non-uniform, particularly under high irradiance when overheating is most pronounced [29,30].

To address these shortcomings, the present study investigates a rear-side cooling design featuring low-power axial fans operating in suction mode. The fans evacuate air from a shallow plenum mounted on the back of the PV module, drawing ambient air through distributed inlet openings and forming multiple impinging jets on the rear surface. This airflow configuration is intended to promote a more uniform temperature field and enhance the overall cooling effect relative to conventional blowing-based arrangements. The suction architecture is compact and compatible with other approaches, such as phase-change materials, offering potential for hybrid thermal management strategies. By reducing both the average temperature and spatial gradients, the proposed system may help mitigate hot-spot formation and support more stable electrical performance under realistic outdoor conditions.

2. Experimental setup

2.1. Test rig design

An experimental rig was developed to assess the performance of the proposed cooling approach applied to a photovoltaic module under actual outdoor operating conditions. The experiments were conducted on two PV panels installed with a tilt angle of 35°, placed adjacent to each other on the rooftop of the Mechanical Engineering Department at Sharif University of Technology, Iran. This

configuration was intended to reduce variations in solar irradiance and to provide similar environmental conditions for both the cooled module and the reference panel.

A rear cooling channel was integrated behind the panel, and four low-power axial fans were mounted at its outlet to induce suction-driven airflow across the backside surface. The channel geometry and fan placement were selected to promote distributed air intake along the rear surface rather than localized forced jets. The panel was evaluated under two configurations: with the fan cooling activated and under a reference condition without airflow. Figure 1 illustrates the outdoor setup, Figure 2 provides a schematic of the cooling system, and Tables 1 and 2 list the specifications of the PV module and the fans, respectively.

Figure 1. Outdoor experimental arrangement of the PV systems

Table 1. Photovoltaic module specifications

Model	BENQ-PM096B00_333
P_m	333W
V_{mp}	54.7V
I_{mp}	6.09A
V_{oc}	64.9V
I_{sc}	6.58A
Dimensions	1559×1046×46mm
Max system voltage	1000 V

The cooling system was evaluated under two operating modes. For the long-term outdoor experiment, the fans operated continuously from 10:00 to 16:00. on September 25, 2025, at the rooftop test site of the Mechanical Engineering Department at Sharif University of Technology. Meteorological conditions during this period are summarized in Table 3. Preliminary tests indicated that approximately 5 minutes of operation were sufficient for the cooled module to approach a lower quasi-steady temperature. In contrast, the temperature recovered toward the reference level within roughly 10 minutes after fan shutdown. At 1 p.m., in a separate thermoelectric test, the fans were controlled cyclically, operating for 5 minutes followed by 10 minutes off, for a 15-minute duty cycle. This intermittent operation was selected to reduce auxiliary energy consumption and to assess the module's transient thermal and electrical responses under periodic cooling.

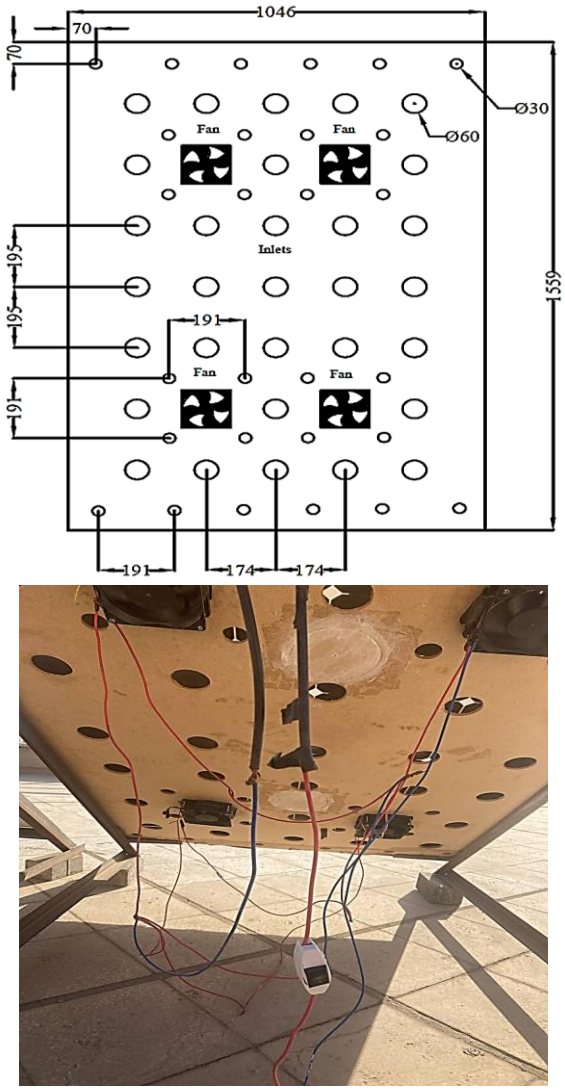

Figure 2. Schematic illustration and photograph of the air-fan cooling configuration

Table 2. Specifications of the fans

Model	PAPST - 4118N/6XMV
Power per fan	4.5W
Speed	3000RPM
Airflow rate	82CFM
Dimensions	120×120×38 mm

2.2. Cooling concept and system description

A sealed plenum chamber was constructed behind the PV module using MDF boards, with a depth of 5 cm to provide a controlled airflow pathway. Instead of conventional blowing fans, the system employs exhaust-mode fans mounted on the rear cover to evacuate warm air from the plenum. This extraction generates a mild under-pressure, drawing ambient air through a series of circular inlet openings (30 and 60 mm in diameter) distributed across the rear surface (Figure 2). The distributed inflow establishes multiple localized cooling streams along the plenum surface before being collected by the fans.

The suction-driven inflow generates localized air streams that enhance rear-surface convection and disrupt stagnant thermal regions. Extracting air from the plenum reduces the tendency for warm-air recirculation, which is frequently observed in backside blowing configurations. The closed plenum constrains airflow through the intended inlet orifices, directing it toward the panel rear surface before the fans collect it. A schematic of the cooling concept is presented in Figure 3.

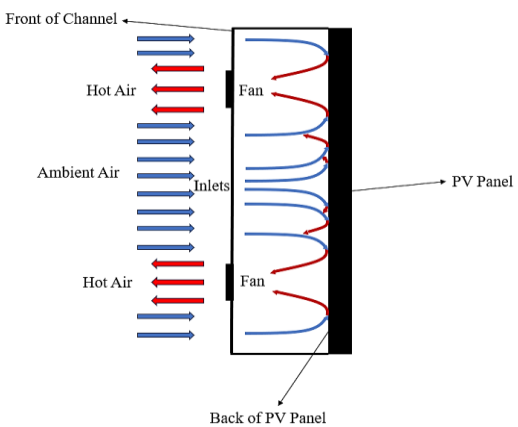

Figure 3. A schematic diagram of the proposed cooling method

During the outdoor tests, the module surface temperature, solar irradiance, ambient temperature, and wind speed were recorded at regular measurement intervals. Infrared images were acquired at selected time points to characterize the spatial temperature distribution across the panel surface. The measured surface temperatures were subsequently combined with the manufacturer-reported temperature coefficient of power. They measured solar irradiance to approximate the electrical performance of the modules, using a methodology commonly adopted in PV thermal studies when direct I-V measurements are unavailable.

To estimate the influence of module temperature on the electrical output of the PV panel, the maximum power was calculated using the relation [31]

$$P_{\max} = P_{\max,ref}\frac{G_T}{G_{T,ref}}\left[1-\gamma(T_c-25)\right] \quad (1)$$

Where Pmax is the maximum power output of the PV module under the actual operating conditions, and Pmax, ref is the maximum power at Standard Test Conditions (STC), i.e., cell temperature of 25°C and $G_{T,ref}$ =1000 W/m2. The coefficient γ is the temperature coefficient of power (−0.33 %/°C, as provided in the module datasheet), and Tc is the average cell (surface) temperature obtained from the thermal measurements. G_T denotes the in-plane solar irradiance measured during the present study. This relation shows that each 1°C increase in cell temperature results in a proportional reduction in power output, with the magnitude of the reduction determined by γ. To quantify the improvement in electrical performance due to the cooling system, the relative increase in electrical energy output was evaluated as [29]

$$\Delta\eta = \frac{E_{cooling}-E_{reference}}{E_{reference}}\times 100 \quad (2)$$

Where $E_{cooling}$ is the total energy output of the fan-cooled PV system, and $E_{reference}$ is the total energy output of the uncooled PV system. The quantity Δη thus represents the percentage increase in electrical output attributed solely to the thermal management strategy.

2.3. Measurement procedure

Surface temperatures were measured using type-K thermocouples. Five thermocouples were mounted on the cooled PV module and five on the reference module to enable a direct comparison of temperature distributions. For each sensor, three readings were taken at every measurement hour, and the values shown in the plots represent the average of these measurements.

In photovoltaic thermal studies, the temperature of the front glass surface is commonly used as an approximation of the cell temperature, as the thermal resistance between the glass and encapsulated cells is small and the transient delay is negligible under steady irradiance. This assumption is valid provided that airflow- and shading-induced spatial gradients are minimal and no hotspots form.

Ambient temperature and wind speed were measured with a Testo 405i hot-wire anemometer, and global solar irradiance was recorded using a TES solar meter positioned adjacent to the experimental setup.

All thermocouples were connected to a BTM-4208SD data logger, which continuously recorded and stored the temperature measurements throughout the experiment. A Seek Thermal infrared camera was also used to acquire thermographic images of the PV module surfaces and to characterize the spatial distribution of surface temperatures. The temperatures derived from infrared imaging agreed with the thermocouple readings to within 1 °C, indicating that the surface measurements reliably reflect the modules' operating temperature under the tested conditions. An overview of the experimental setup is provided in Figure 4.

Table 3. PV module parameters considered in the case study

Date	25/9/2025
Solar radiation	1030W/m^2
The ambient temperature	32°C
Wind speed	3.96Km/hr

Figure 4. The overall experimental setup

2.4. Uncertainty analysis

2.4.1. Temperature uncertainty

The surface temperature of the PV module was continuously monitored through five type-K thermocouples attached to the front face of the panel. For each thermocouple, three consecutive readings were recorded at each measurement interval. The average temperature of each thermocouple was calculated from its three measurements, and the panel surface temperature was then determined as the arithmetic mean of the five individual thermocouple averages.

The uncertainty associated with the measured panel temperature consists of two independent components: (i) the repeatability of the thermocouple readings and (ii) the instrumental uncertainty. The repeatability uncertainty of each thermocouple was obtained from the sample standard deviation of the three readings, and these contributions were statistically propagated to the panel-level mean across the five sensors. The instrumental uncertainty of each type-K thermocouple was taken as ±0.1°C based on the manufacturer's specification. Since the thermocouples operate as independent sensors, the instrumental error decreases by a factor of $\sqrt{5}$ when averaged across the panel.

The combined standard uncertainty of the panel surface temperature was calculated using the root-sum-of-squares (RSS) method

$$u_T = \sqrt{u^2_{rep,panel} + u^2_{tc,panel}} \quad (3)$$

Where $u_{rep,panel}$ is the repeatability contribution of the five thermocouples to the panel mean, and $u_{tc,panel}$ is the thermocouple accuracy contribution to the averaged surface temperature. Based on the experimental data, the combined standard uncertainty of the measured PV surface temperature, with a coverage factor k=2 for a 95% confidence level, is 0.15°C.

In addition, using Eq. (3), the uncertainty associated with measuring the temperature difference between the inlet and outlet air behind the photovoltaic panel, as measured by an anemometer, was evaluated. With a coverage factor of k=2, the expanded uncertainty of the temperature difference was determined to be 0.59 °C.

2.4.2. Output power uncertainty

The uncertainty in the calculated electrical power was evaluated using the uncertainty propagation method proposed by Moffat [32]. Since the electrical power depends on several measured quantities, the

total uncertainty was obtained by combining the individual contributions of the relevant parameters. The method accounts for the sensitivity of the output variable to each input through partial derivatives. It aggregates the effects of the measurement uncertainties using a root-sum-of-squares formulation. Since the electrical power output, according to Eq. (1), is a function of the PV surface temperature and solar irradiance, its uncertainty was evaluated using the propagation expression

$$u_P = \sqrt{(\frac{\partial P}{\partial T})^2 (u_T)^2 + (\frac{\partial P}{\partial G})^2 (u_G)^2} \quad (4)$$

Where u_T and u_G denote the uncertainties of the surface temperature and the solar irradiance, respectively. Based on the measured uncertainties of the relevant input variables, the combined uncertainty of the calculated electrical power was determined to be 1.97%.

Table 4. Instrument measurement uncertainty

Instrument	Uncertainty
Solar meter	±10W/m^2
Hot wire anemometer	±0.5°C-0.17m/s
Thermocouples type K	±0.1°C
Infrared camera	±0.3°C

3. Results and discussion

3.1. Climatic data

To examine the thermal performance of the developed cooling system under real operating scenarios, experimental tests were performed on a clear day during the period from 10 a.m. to 4 p.m. Figure 5 illustrates the variations in ambient temperature, solar irradiance, and the wind-speed profile during the testing period. The ambient temperature increased gradually in the morning, reaching a peak of approximately 32 °C around midday, then decreased slightly toward the afternoon. Similarly, solar irradiance rose steadily from the beginning of the test, reaching a maximum of approximately 1030 W/m² near solar noon, followed by a moderate decline in the late afternoon. The ambient wind speed was about 3.96 Km/hr, with modest intra-day fluctuations; this parameter is particularly relevant as it influences the external convective heat-transfer coefficient on the panel surfaces and, consequently, the cooling effectiveness. Such variations in weather conditions are critical, as ambient temperature, solar intensity, and wind speed directly affect the surface temperature of photovoltaic panels and their cooling effectiveness. Therefore, monitoring these parameters ensures the reliability and consistency of the comparative analysis between the cooled and uncooled panels.

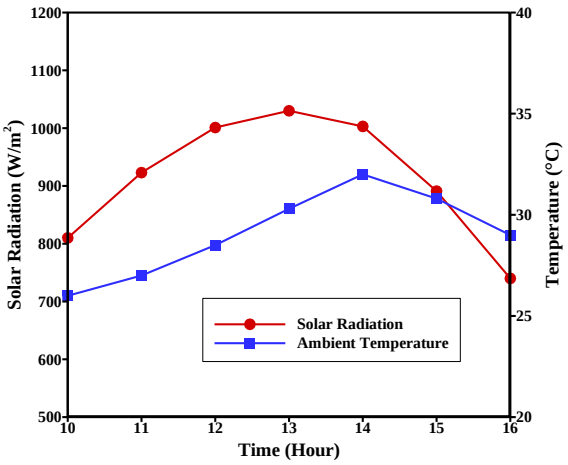

(a)

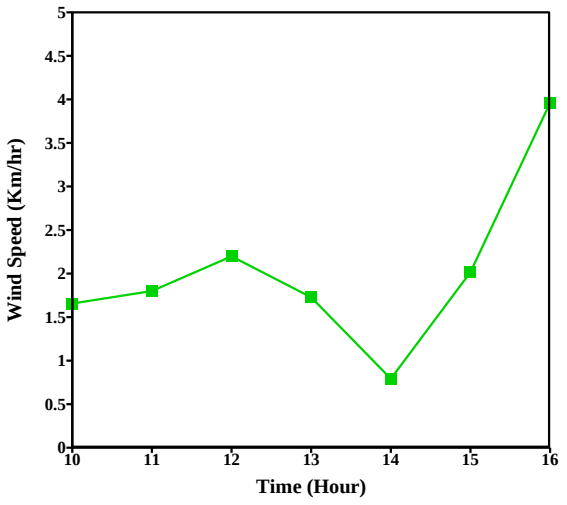

(b)

Figure 5. (a) Changes in ambient temperature and solar irradiance with time in Tehran, (b) Variation of wind speed with time in Tehran

3.2. Thermal performance

Figure 6 depicts the temporal profile of the PV modules' average surface temperature during the period from 10:00 to 16:00. Both panels followed the expected daytime trend, increasing toward solar noon and decreasing afterward; however, the cooled module consistently operated at a lower temperature. At peak irradiance (1 p.m.), the reference panel

reached 56.4°C, whereas the suction-cooled panel remained at 40.9 °C, yielding a maximum difference of 15.5 °C. This temperature gap persisted throughout the test window, indicating that the rear-side suction configuration limited heat accumulation on the module surface under outdoor conditions. The reduced temperature variation suggests a more stable thermal response during irradiance fluctuations, with the largest difference occurring at high solar intensities.

Infrared thermal images captured at 1 p.m., when the modules reached their maximum operating temperature, provide a spatial assessment of the cooling performance (Figure 7). The cooled panel displays a uniform temperature field of 39-41 °C with no visible high-temperature regions, whereas the reference module remains within the 54-56 °C range and exhibits several localized hot spots in its central area. Such gradients are known to induce differential thermal stresses and can accelerate degradation in crystalline silicon modules. The infrared readings were consistent with the thermocouple measurements within less than 1 °C, supporting the use of surface temperatures as a representative indicator of module operating temperature under the tested conditions. Under these circumstances, the suction-based cooling system achieved a maximum reduction of approximately 15.5°C and substantially reduced in-plane temperature non-uniformities associated with hot-spot formation.

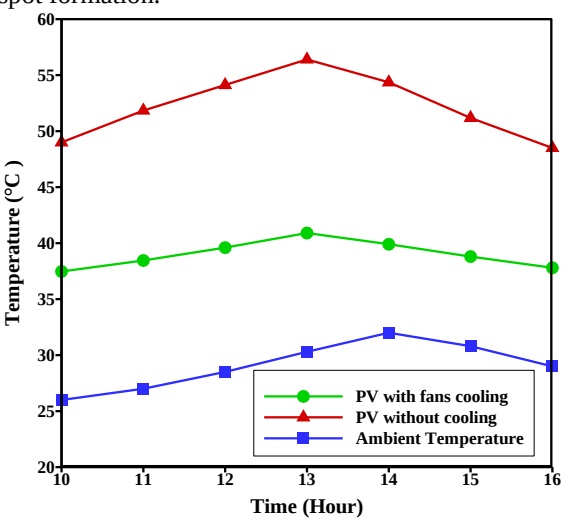

Figure 6. Time-dependent comparison of ambient and average PV temperatures

To quantify the heat removal capability of the airflow, the temperature difference ($\Delta T=T_{out}-T_{in}$) between the air inlet and outlet of the cooling channel was measured throughout the day (Figure 8). The air outlet temperature consistently exceeded the air inlet temperature, confirming continuous heat transfer from the module to the moving air. The temperature difference increased during periods of high irradiance, indicating that the system removed more heat when thermal loading was highest, which aligns with the observed improvement in panel temperature and uniformity.

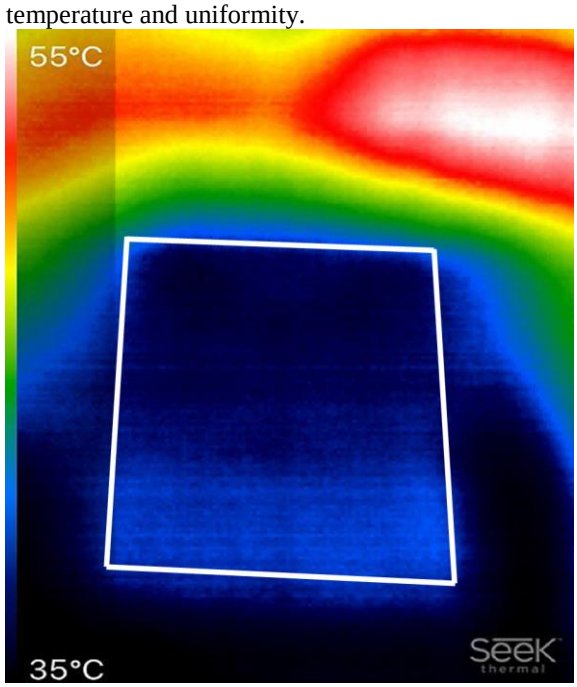

(a)

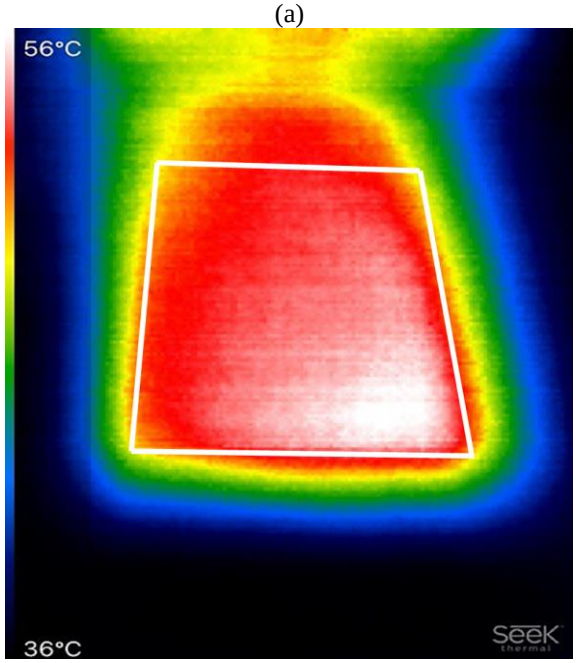

(b)

Figure 7. Infrared thermal image of the (a) PV panel with cooling, (b) PV panel without cooling

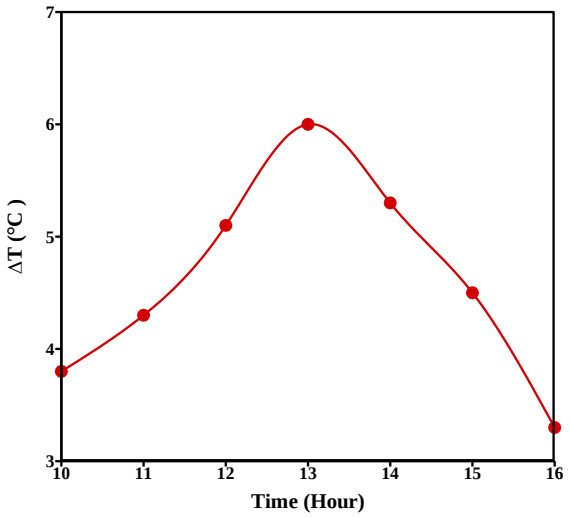

Figure 8. The temperature difference between the air entering the cooling channel and the air discharged from the fans

According to Figure 8, the air temperature difference between the inlet and outlet was 3.8 °C at 10:00, corresponding to the relatively low irradiance in the early period. A steady increase in the temperature difference was observed as solar radiation approached its midday maximum, reaching 6.0 °C at 13:00, coinciding with the period of highest surface heating. This increase reflects a larger amount of thermal energy being transferred to the airflow. Following the afternoon decline in irradiance, the temperature difference decreased to 3.3 °C by 16:00.

The variation in the inlet-outlet air temperature difference suggests a sensitivity of the cooling process to solar intensity. Larger temperature differences were observed at higher irradiance levels, indicating that a greater amount of thermal energy was removed by the airflow during periods of elevated module heating. This trend is consistent with the peak reduction observed in the module surface temperature near solar noon.

In photovoltaic-powered desalination systems, such as humidification-dehumidification (HDH) units, the outlet airflow extracted from the PV backside can be used as a thermal input. Since this air stream consistently leaves the cooling channel at a higher temperature than the ambient intake temperature, it can be introduced into the HDH process to enhance evaporation efficiency and improve overall system performance. Therefore, the proposed cooling configuration not only stabilizes the module's electrical output but also provides a secondary thermal resource that can increase the operational efficiency of HDH desalination systems.

3.3. Electrical performance

The electrical performance was evaluated by combining the measured surface temperatures with the manufacturer's temperature coefficient of power and measured solar irradiance, as no direct I-V measurements were recorded. Figure 9 shows the evolution of the instantaneous power output of both modules over a 15-minute duty cycle. The adopted 15-minute protocol was intentionally selected to capture the transient coupling between backside heat extraction and PV electrical response, including surface stabilization, hotspot suppression, and auxiliary energy overhead, rather than to evaluate full-day energy yield. As such, the integrated power values should be interpreted as short-term performance indicators under realistic outdoor conditions.

Under nearly constant irradiance, the cooled panel exhibited a higher power output throughout the cycle. When the fans were switched on, the output of the cooled module increased from 301.11 W at t = 0 min to 325.1 W at t = 5 min, whereas the reference module remained below this level for the entire period. After the fans were switched off, the power of the cooled panel gradually decreased due to thermal inertia but remained consistently above that of the uncooled reference. This behavior is consistent with the underlying semiconductor physics: a reduction in surface temperature mitigates junction-level recombination. It enhances carrier mobility, resulting in a modest increase in output power under steady irradiance.

Integration of the power-time curves over the 15-minute interval is summarized in Table 5. The reference module generated 82.1 Wh, while the cooled module produced 84.4 Wh, corresponding to a 2.8% gross electrical gain. The auxiliary power consumption of the four fans during the 5-minute cooling phase was 1.5 Wh, leading to a net energy of 82.9 Wh and an effective electrical improvement of 0.94%. The difference between gross and net gain reflects the inherent overhead of the cooling system: while active extraction increases instantaneous electrical output, it also consumes energy during operation.

The electrical efficiency enhancement reported in this study was obtained using the manufacturer's

temperature coefficient (γ), derived from the measured reduction in PV surface temperature and measured solar irradiance. Since direct I-V data were unavailable during the experimental period due to seasonal irradiance limitations, the results represent an estimate of the expected electrical gain rather than the actual electrical output, a widely accepted practice in PV thermal studies when direct electrical characterization is not feasible.

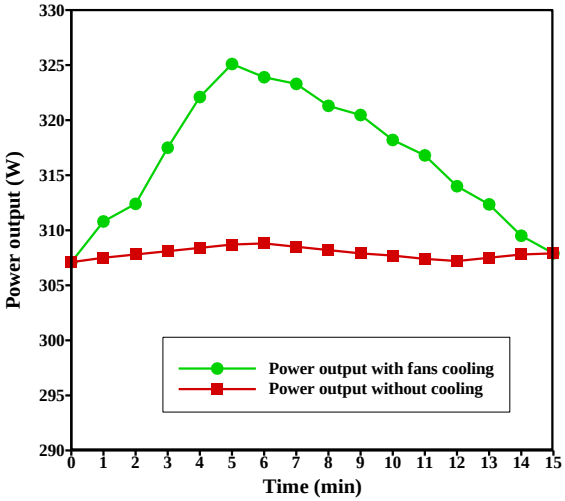

Figure 9. Time variation of PV panel output power with and without cooling during a 15-min interval

Table 5. Total energy during 15 min at the Cooled and uncooled photovoltaic panels

Energy generation and consumption	Energy (Wh)
Total energy output of the uncooled PV system	82.1
Total energy output of the fan-cooled PV system	84.4
Energy consumed by fans	1.5
Net energy with fan cooling	82.9

3.4. Comparative Analysis with Previous Cooling Approaches

To better demonstrate the effectiveness of the proposed cooling approach, the results were compared with those reported in previous studies that employed different cooling strategies, including both fan-based active cooling and free convection methods. Table 6 summarizes the maximum reductions in surface temperature and improvements in electrical efficiency achieved in these works, along with those of the present study.

As a comparison, Hussien et al. [29] employed eight rear-mounted fans operating in blowing mode with a total power consumption of 18.4 W, which is higher than the auxiliary power required by the fans used in the present study. Their configuration achieved a surface temperature reduction of 9.9°C; however, noticeable temperature gradients remained across the photovoltaic panel surface. In contrast, the present work employs four fans operating in suction mode, combined with a distributed airflow design, resulting in a maximum surface temperature reduction of 15.5°C and an almost uniform temperature distribution over the panel surface. These results indicate the superiority of the suction-based cooling architecture adopted in this study compared to conventional blowing-based fan cooling configurations.

According to Table 6, although the suction-based configuration achieved the largest average temperature reduction among the compared studies, the resulting electrical improvement remained modest. This is because distributed airflow extraction produces a uniform thermal field across the PV surface, suppressing hotspots and minimizing local gradients without inducing sharp perturbations in Imp or V_{mp}. Conversely, cooling technologies based on jet impingement, fins, or heat pipes generate localized low-temperature regions that drive transient increases in MPP parameters, leading to higher reported electrical gains despite lower overall temperature reductions. In contrast, the uniform cooling profile obtained in the present work stabilizes the module's I-V characteristics, yielding smoother power trajectories and eliminating sudden spikes in output that typically arise from aggressive, highly concentrated cooling.

By mitigating hotspot formation and reducing differential thermal stresses between adjacent cells, the suction system prevents microcrack initiation, solder fatigue, and delamination of encapsulation layers, factors that are well known to accelerate performance degradation. Therefore, despite the more moderate short-term electrical gain, the proposed distributed cooling strategy promotes long-term reliability, operational stability, and healthier semiconductor junction behavior, which are essential for sustained PV performance under real outdoor conditions.

Table 6. Comparative analysis of the present study with previous works

References	Cooling method	Maximum temperature reduction (°C)	Electrical efficiency improvement (%)
Shahsavar et.al [30]	PV/T air collector with 8 fans (forced convection)-52.8 W required power	< 8	7
Badi et.al [11]	PCM	5-6	3
Krstic et.al [5]	Heat sink	7.5	-
Praveenkumar et.al [6]	Heat pipe	6.72	2.98
Hussien et.al [29]	Forced air convection with 8 fans, 18.4 W required power	9.9	7
Present study	Forced air convection with 4 fans, 18 W required power	15.5	0.94

4. Conclusion

This study experimentally evaluated a suction-based fan cooling system for rear-side thermal management of photovoltaic modules under real outdoor conditions. In this configuration, low-power axial fans extract air from a shallow plenum, promoting distributed inflow across the rear surface. The system achieved a maximum surface-temperature reduction of 15.5 °C at peak irradiance. Infrared thermography indicated a substantially more uniform temperature field on the cooled module, with no visible hot spots at the time of observation, in contrast to the non-cooled panel.

The electrical analysis showed that, during a 15-minute duty cycle, the cooled module delivered 84.4 Wh compared with 82.1 Wh for the reference module, resulting in a 2.8% gross gain. After accounting for auxiliary fan consumption of 1.5 Wh, the net improvement in electrical output was estimated at 0.94%. Although this net gain is relatively small, the cooling configuration concurrently reduced both the average surface temperature and the spatial thermal gradients, which may help limit temperature-induced stresses and contribute to more stable operating conditions.

In this study, the I-V characteristics of the photovoltaic module were not directly measured, and the output power was estimated using temperature-based performance correlations. This limitation may affect the accuracy of the electrical performance evaluation and should be addressed in future investigations through direct I-V measurements. The suction-based configuration is compact, requires low auxiliary power, and can be integrated with other cooling strategies, such as phase-change materials or PV/T systems, enabling hybrid thermal management approaches. Future work should extend the outdoor experiments over longer operating periods, include direct I-V characterization to quantify electrical performance, and examine the influence of fan arrangement and plenum geometry on thermal behavior and energy yield.

Nomenclature

$E_{cooling}$	Total energy generated for PV with cooling (Wh)
$E_{reference}$	Total energy generated in the noncooled PV panel (Wh)
G_T	Solar radiation (W/m^2)
$G_{T,\,ref}$	Solar radiation at Standard Test Conditions (1000 W/m^2)
I	Current (A)
I_{mp}	Current at maximum power (A)
I_{sc}	Short-circuit current (A)
k	Coverage factor
P	Power (W)
P_{max}/P_m	Max power output (W)
$P_{max,\,ref}$	Maximum power at Standard Test Conditions (W)
STC	Standard test condition
T	Temperature (°C)
T_c	PV cell temperature (°C)
T_{in}	Air inlet temperature (°C)
T_{out}	Air outlet temperature (°C)
ΔT	Temperature difference (°C)

u_P	Power Uncertainty (%)
u_T	Temperature Uncertainty Difference (%)
u_G	Irradiation Uncertainty Difference (%)
$u_{rep,panel}$	Repeatability Uncertainty (%)
$u_{tc,panel}$	Thermocouple Uncertainty (%)
V	Voltage (V)
V_{mp}	Voltage at maximum power (V)
V_{oc}	Open circuit voltage (V)
η	Energy efficiency (%)
γ	Temperature coefficient (%/°C)

References

[1] A. R. Elbakheit, S. Waheeb, and A. Mahmoud, "A Ducted Photovoltaic Façade Unit with Forced Convection Cooling," *Sustainability*, vol. 14, no. 19, p. 12875, 2022, doi: https://doi.org/10.3390/su141912875.

[2] S. Sharma, N. Sellami, A. A. Tahir, T. K. Mallick, and R. Bhakar, "Performance improvement of a CPV system: experimental investigation into passive cooling with phase change materials," *Energies*, vol. 14, no. 12, p. 3550, 2021, doi: https://doi.org/10.3390/en14123550.

[3] K. Sornek, W. Goryl, R. Figaj, G. Dąbrowska, and J. Brezdeń, "Development and tests of the water cooling system dedicated to photovoltaic panels," *Energies*, vol. 15, no. 16, p. 5884, 2022, doi: https://doi.org/10.3390/en15165884.

[4] E. Abdelsalam, H. Alnawafah, F. Almomani, A. Mousa, M. Jamjoum, and M. Alkasrawi, "Efficiency improvement of photovoltaic panels: A novel integration approach with cooling tower," *Energies*, vol. 16, no. 3, p. 1070, 2023, doi: https://doi.org/10.3390/en16031070.

[5] M. Krstic *et al.*, "Passive cooling of photovoltaic panel by aluminum heat sinks and numerical simulation," *Ain Shams Eng. J.*, vol. 15, no. 1, p. 102330, 2024, doi: https://doi.org/10.1016/j.asej.2023.102330.

[6] S. Praveenkumar *et al.*, "Experimental study on performance enhancement of a photovoltaic module incorporated with CPU heat pipe—A 5E analysis," *Sensors*, vol. 22, no. 17, p. 6367, 2022, doi: https://doi.org/10.3390/s22176367.

[7] S. V. Hudişteanu, F. E. Țurcanu, N. C. Cherecheș, C. G. Popovici, M. Verdeș, and I. Huditeanu, "Enhancement of PV panel power production by passive cooling using heat sinks with perforated fins," *Appl. Sci.*, vol. 11, no. 23, p. 11323, 2021, doi: https://doi.org/10.3390/app112311323.

[8] A. Alqatamin, O. A. Al-Khashman, and J. Su, "A Novel Heatsink for Optimizing Photovoltaic Cell Performance With Passive Cooling Using Perforated Wave-Shaped Fins," *J. Sol. Energy Eng.*, vol. 147, no. 5, p. 51002, 2025, doi: https://doi.org/10.1115/1.4068410.

[9] M. F. Jaffar, A. T. Mohammad, A. Q. Ahmed, and W. A. M. Al-Shohani, "Experimental investigation of using the evaporative air cooling technique to enhance the performance of the photovoltaic module," *Int. J. Low-Carbon Technol.*, vol. 19, pp. 1231–1245, 2024, doi: https://doi.org/10.1093/ijlct/ctae067.

[10] A. Durez, M. Ali, A. Waqas, K. Nazir, and S. Kumarasamy, "Modelling and optimization of phase change materials (PCM)-based passive cooling of solar PV panels in multi climate conditions," *Front. Energy Res.*, vol. 11, p. 1121138, 2023, doi: https://doi.org/10.3389/fenrg.2023.1121138.

[11] N. Badi, S. A. Alghamdi, H. M. El-Hageen, and H. Albalawi, "Onsite enhancement of REEEC solar photovoltaic performance through PCM cooling technique," *PLoS One*, vol. 18, no. 3, p. e0281391, 2023, doi: https://doi.org/10.1371/journal.pone.0281391.

[12] A. Al Miaari and H. M. Ali, "A recent review on thermal management of photovoltaic panels using phase change material based on thermal conductivity enhancers for sustainable buildings," *J. Energy Storage*, vol. 103, p. 113936, 2024, doi: https://doi.org/10.1016/j.est.2024.113936.

[13] I. Čorić, S. Nižetić, and M. Jurčević, "Progress in passive cooling strategies for silicon photovoltaic panels with incorporated phase change materials," *Energy*, p. 136370, 2025, doi: https://doi.org/10.1016/j.energy.2025.136370.

[14] F. Wang *et al.*, "Enhancing heat transfer of photovoltaic panels with fins," *Int. J. Energy Res.*, vol. 2024, no. 1, p. 5180627, 2024, doi: https://doi.org/10.1155/2024/5180627.

[15] T. Ibrahim, F. Hachem, M. Ramadan, J. Faraj, G. El Achkar, and M. Khaled, "Cooling PV panels by free and forced convections: Experiments and comparative study.," *AIMS Energy*, vol. 11, no. 5, 2023, doi: https://doi.org/10.3934/energy.2023038.

[16] S.-V. Hudișteanu, N.-C. Cherecheș, F.-E. Țurcanu, I. Hudișteanu, M. Verdeș, and A.-D. Ancaș, "Experimental analysis of innovative perforated heat sinks for enhanced photovoltaic efficiency," *Energy Convers. Manag. X*, vol. 25, p. 100842, 2025, doi: https://doi.org/10.1016/j.ecmx.2024.100842.

[17] V. S. Poddar, V. A. Ranawade, and N. B. Dhokey, "Study of synergy between photovoltaic, thermoelectric and direct evaporative cooling system for improved performance," *Renew. Energy*, vol. 182, pp. 817–826, 2022, doi: https://doi.org/10.1016/j.renene.2021.10.040.

[18] P. Bevilacqua, S. Perrella, D. Cirone, R. Bruno, and N. Arcuri, "Efficiency improvement of photovoltaic modules via back surface cooling," *Energies*, vol. 14, no. 4, p. 895, 2021, doi: https://doi.org/10.3390/en14040895.

[19] A. M. Elbreki, F. Mohamed, W. Elbsuoni, and M. Elmnif, "Active cooling of PV module performance enhancement using air duct with fans: Indoor Experimental Study," in *The 7th International Conference on Engineering & MIS 2021*, 2021, pp. 1–5. doi: https://doi.org/10.1145/3492547.34925.

[20] B. R. Utomo, A. Sulistyanto, T. W. B. Riyadi, and A. T. Wijayanta, "Enhanced Performance of Combined Photovoltaic–Thermoelectric Generator and Heat Sink Panels with a Dual-Axis Tracking System," *Energies*, vol. 16, no. 6, p. 2658, 2023, doi: https://doi.org/10.3390/en16062658.

[21] A. Saxena, N. Agarwal, and B. Norton, "Design and performance characteristics of an innovative heat sink structure with phase change material for cooling of photovoltaic system," *Energy Sources, Part A Recover. Util. Environ. Eff.*, vol. 47, no. 1, pp. 10721–10745, 2025, doi: https://doi.org/10.1080/15567036.2021.1968545.

[22] K. Appalasamy, R. Mamat, and S. Kumarasamy, "Smart thermal management of photovoltaic systems: Innovative strategies," *AIMS Energy*, vol. 13, no. 2, pp. 309–353, 2025, doi: https://doi.org/10.3934/energy.2025013.

[23] M. Alktranee and P. Bencs, "Experimental comparative study on using different cooling techniques with photovoltaic modules.," *J. Therm. Anal. Calorim.*, vol. 148, no. 9, 2023, doi: https://doi.org/10.1007/s10973-022-11940-1.

[24] L. Jyani, S. K. Sankhala, K. Chaudhary, and K. Purohit, "Experimental Investigation of Flexible Solar Cells Using Passive Cooling Technique in Hot and Dry Climate of Jodhpur," *J. Sol. Energy Res.*, vol. 9, no. 2, pp. 1854–1869, 2024, doi: 10.22059/jser.2024.371686.1376.

[25] P. Dwivedi, K. Sudhakar, A. Soni, E. Solomin, and I. Kirpichnikova, "Advanced cooling techniques of PV modules: A state of art," *Case Stud. Therm. Eng.*, vol. 21, p. 100674, 2020, doi: https://doi.org/10.1016/j.csite.2020.100674.

[26] M. Sharaf, M. S. Yousef, and A. S. Huzayyin, "Review of cooling techniques used to enhance the efficiency of photovoltaic power systems," *Environ. Sci. Pollut. Res.*, vol. 29, no. 18, pp. 26131–26159, 2022, doi: https://doi.org/10.1007/s11356-022-18719-9.

[27] O. A. A.-M. Ibrahim, S. A. Kadhim, and M. K. S. Al-Ghezi, "Photovoltaic panels cooling technologies: Comprehensive review," *Arch. Thermodyn.*, vol. 44, no. 4, pp. 581–617, 2023, doi: 10.24425/ather.2023.149720.

[28] A. Al Miaari and H. M. Ali, "Technical method in passive cooling for photovoltaic panels using phase change material," *Case Stud. Therm. Eng.*, vol. 49, p. 103283, 2023, doi: https://doi.org/10.1016/j.csite.2023.103283.

[29] A. Hussien, A. Eltayesh, and H. M. El-Batsh, "Experimental and numerical investigation for PV cooling by forced convection," *Alexandria Eng. J.*, vol. 64, pp. 427–440, 2023, doi: https://doi.org/10.1016/j.aej.2022.09.006.

[30] A. Shahsavar and M. Ameri, "Experimental investigation and modeling of a direct-coupled PV/T air collector," *Sol. Energy*, vol. 84, no. 11, pp. 1938–1958, 2010, doi: https://doi.org/10.1016/j.solener.2010.07.010.

[31] M. Fuentes, G. Nofuentes, J. Aguilera, D. L. Talavera, and M. Castro, "Application and validation of algebraic methods to predict the behaviour of crystalline silicon PV modules in Mediterranean climates," *Sol. Energy*, vol. 81, no. 11, pp. 1396–1408, 2007, doi: https://doi.org/10.1016/j.solener.2006.12.008.

[32] R. J. Moffat, "Describing the uncertainties in experimental results," *Exp. Therm. fluid Sci.*, vol. 1, no. 1, pp. 3–17, 1988, doi: https://doi.org/10.1016/0894-1777(88)90043-X.